Scientific Frontiers in Research on Extrasolar Planets
ASP Conference Series, Vol. 294, 2003
D. Deming and S. Seager, eds.

Imaging Extrasolar Planets From the Ground

Roger Angel

Steward Observatory, 933 N. Cherry Ave, Tucson, AZ 85721

Abstract. An approach to direct imaging of extrasolar planets is described, in which adaptive optics to correct atmospheric aberration are based on interferometric measurements made in the focal plane. In order to minimize the weak, residual speckles of the stellar halo, their complex amplitudes are first determined using photon-counting, spectrally-resolved imaging sensors. Corrections to both the corrugation and intensity of the wavefront are then derived by Fourier transform and applied using a pair of deformable mirrors. In this way the systematic and non-common path errors of pupil wavefront sensing methods are avoided, and the resulting high accuracy correction should allow detection of giant extrasolar planets with existing large telescopes. With new ground-based telescopes of ~ 20 m or larger aperture, detection and even spectroscopy of nearby earth-like planets should be possible.

1. Introduction

No telescope currently has the sensitivity to image extrasolar planets. For ground-based systems the limitation is not fundamental, but arises because the adaptive optics (AO) currently in use are generally optimized for wavefront measurements of relatively faint natural guide stars and permit only moderate correction accuracy. Faint sub-stellar companions are detected (Close et al. 2002), but the residual halo of uncorrected light (containing typically about half the stellar flux) prevents detection when the contrast ratio is high. The situation is illustrated in Figure 1, showing a 10 second exposure of a bright calibration star obtained with the Keck telescope with adaptive optics. The marked binary companion 0.65 arcsec from the star and $2500\times$ fainter is clearly visible. But the remaining star-like features result from small, uncorrected, quasi-static optical aberrations. If this image were of a twin of the solar system at 10 pc, even Jupiter, at 0.5 arcsec separation and intensity 10^{-9} of the star, would be $100,000\times$ fainter than these speckles.

Adaptive optics correction would be much better if full advantage were taken of bright star fluxes to more accurately measure and correct atmospheric distortion and static errors. In principle, even a 6.5 m telescope, by averaging long exposures, could be used to image the jupiter in a solar system twin at 8 pc (Angel 1994; Stahl and Sandler 1995). A planet like Earth, however, 5 times closer-in and ~ 8 times fainter ($1.5 \times 10^{-10}$of the star), is still more difficult. In the following analysis I explore the potential to meet these challenges, given

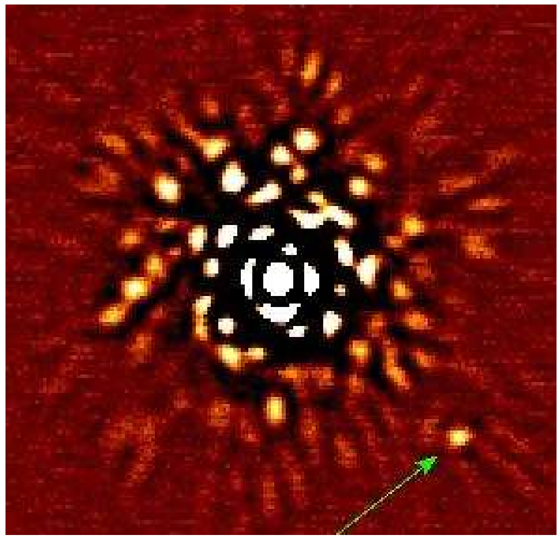

Figure 1. Image of a V=8 magnitude star at 1.56 μm wavelength made with the Keck AO facility with the NIRC-2 IR AO camera. To minimize speckle structure, a pupil mask was used to create a 9m circular wavefront. The radially averaged PSF has been subtracted. Courtesy William Merline & Laird Close, and the Keck Observatory.

rapid wavefront corrections derived from measurements of the residual starlight halo rather than from conventional pupil measurements.

2. A Strategy for Measuring Residual Wavefront Errors

2.1. Character of the Halo When Wavefront Errors are Small

The intensity of the focal plane halo at a point $\boldsymbol{\theta}$ from the star varies as the square of the complex probability amplitude a$(\boldsymbol{\theta}, \lambda)$, given by the Huygens-Fresnel integral over the pupil (Born, Woolf and Bhatia 1999). If AO correction of the corrugation z and intensity I (scintillation) of the bright star wavefront results in errors Δz($\mathbf{x}$) and ΔI($\mathbf{x}$) across the pupil that are both small, i.e. $2\pi\Delta z/\lambda$ and $\Delta I/I \ll 1$, then the ratio of halo amplitude at $\boldsymbol{\theta}$ to that of the central star is given by

$$\frac{a(\boldsymbol{\theta},\lambda)}{a(0,\lambda)} = \int e^{2\pi i\boldsymbol{\theta}\cdot\mathbf{x}/\lambda} T(\mathbf{x}) \left(1 + \frac{\Delta I(\mathbf{x})}{2I} + \frac{2\pi i \Delta z(\mathbf{x})}{\lambda}\right) d\mathbf{x}. \quad (1)$$

Here $T(\mathbf{x})$ is the pupil transmission which will be a smoothly tapered apodization function (Jacquinot & Roizen-Dossier 1964) chosen to minimize diffraction in the region of the planet. Let us suppose that suppression adequate for our purpose is achieved at a large telescope by a coronagraph with field and pupil stops, with $\int T(\mathbf{x}) exp(2\pi i\boldsymbol{\theta}\cdot\mathbf{x}/\lambda) d\mathbf{x} \cong 0$ for $\theta > 5\lambda/D$ and unity for $\theta = 0$.

Residual atmospheric aberrations have variable Fourier components that are random and uncorrelated, and when integrated across the pupil would lead to a weak but markedly speckled and changing halo. The speckles formed in white light show systematic radial extension with wavelength, since amplitude depends mostly on $\boldsymbol{\theta}/\lambda$. One successful strategy for distinguishing faint stellar companions takes advantage of this property. The companion is revealed when speckled halo images recorded simultaneously at adjacent wavelengths are radially scaled and subtracted (Racine et al. 1999). However, even in the limit of perfect subtraction, photon noise remains and will set a limit to sensing faint extrasolar planets. To reduce this noise, we must minimize the halo flux by measuring and correcting the wavefront intensity and corrugation to the limits set by photon noise in the wavefront measurement.

2.2. How Best to Measure the Residual Errors

In current and proposed AO techniques, the residual aberration is derived from measurements across the pupil of wavefront phase, slope or curvature (Angel 1994; Roddier 1999). While high accuracy is in principle possible for bright stars, it will be extraordinarily difficult to obtain in practice by these methods for the following reasons. The wavefront aberration will have fine structure arising from variable atmospheric turbulence and, in the case of segmented large mirrors, sharp phase steps at the segment boundaries. These will change with temperature, orientation and wind gusts. Detailed *correction* of high frequency residual errors $\Delta z(\mathbf{x})$ and $I(\mathbf{x})$ with the deformable mirrors is not necessary to minimize the halo very close to the star, which is determined by the low-order Fourier components through Equation 1. Nevertheless, detailed and accurate *measurement* of the wavefront will be needed if these components are to be accurately calculated. Because extrasolar planets are so faint, calibration and freedom from systematic errors would be required to levels far beyond current experience either at the telescope or in the optics shop. The task will be further complicated by unsensed differences in the optical paths to the wavefront sensor and the science camera, resulting in time-variable wavefront errors that could be removed only by repeated calibration to the required exquisite accuracy.

These difficulties can be overcome if the residual wavefront errors are derived from the focal plane image itself, from measurements of the complex amplitude $a(\boldsymbol{\theta}, \lambda)$ across the halo. There are three major advantages to this approach. First, no matter the fine details of the wavefront errors and the compensating deformable mirror shapes, the required corrective pupil Fourier components are given directly. Second, the need for very accurate calibration and measurement is removed because the error measurement is inherently null – there is no signal if there is no error. Third, non-common path errors are eliminated.

Note that the correction based on the focal plane image cannot suppress the planet image, because it is not coherent with the star. Long exposure images to bring out planetary companions thus do not require a separate “science camera.” They can be obtained simply by digitally summing over phase and wavelength many of the short exposures used for phase detection. The AO correction is then closed completely about the recorded halo. Additional images at wavelengths longer than the sensing band may also be obtained with an auxiliary camera, as discussed below.

Focal plane measurements to derive wavefront errors, in the form of phase diversity measurements, were used to determine the correction for the Hubble Space Telescope (Roddier & Roddier 1993). But while the Hubble data were obtained over months with high signal-to-noise ratio in narrow wavelength bands, our measurements to still higher accuracy must be based on measurements of very faint, broadband speckles made in a fraction of a millisecond.

2.3. Focal Plane Interferometer

We propose to derive the wavefront errors from measurements of the complex amplitude of the weak speckled halo. The bright center of the PSF will be blocked by a field stop, with some light from the Airy core reserved to form reference beams for the white light interferometer. Laser-based interferometers that measure complex amplitude or phase are standard equipment for testing in the optical shop, although generally used in the pupil plane. Those closest to our need provide four simultaneous images encoding complete phase data in a single short exposure, using polarization methods to separate phase (Smythe & Moore 1984). For our application where high throughput is critical, we can obtain all four images in unpolarized white light with the configuration shown in Figure 2, which combines interferometer and coronagraph optics.

The pierced mirror in the telescope's AO-corrected focal plane acts as a field stop, reflecting the search field around the star and transmitting the central peak for phase reference. Four relayed images of the annular field are formed via Lyot stops and beamsplitters. With an achromatic 90^o path difference between the two reference beams introduced at semi-transparent mirrors, the four images are combined with reference beams of phases $\phi= 0$, $\pi/2$, π and $3\pi/2$. Transmission elements coated with a film of variable density are included in reference path to balance amplitudes of the interfering beams. The signal/noise ratio for photon noise limited wavefront measurement is maximized when the local reference flux is somewhat brighter than the halo. However, when the planet is to be detected against the noise from the combined halo and reference fluxes, overall sensitivity will be optimized if the reference flux is matched locally to the average radial halo intensity $\langle I(\theta, \lambda)\rangle$ under the prevailing conditions.

For a large telescope of, say, 30 m aperture operating at 1 μm wavelength, halo images out to > 0.1 arcsec search radius correspond to $\theta \sim 25\lambda/D$. The speckles must be recorded with spectral resolution $2D\theta/\lambda \sim$ 50 to prevent spectral blurring, using photon counting detectors to accommodate very low light levels. Photon counting arrays of superconducting tunnel junction elements (STJs) would be ideal detectors because of their high efficiency and inherent spectral resolution, which for hafnium elements could reach the desired level (Perryman & Peacock 2000). But even if STJ technology is not developed in time, today's photon counting array detectors could be used with integral field units (IFUs) (Murphy et al. 2000; Thatte et al. 2000) to provide the required spectral resolution.

With IFUs the detected fluxes will be very low. Allowing for Nyquist sampling for each wavelength in each of four phase images, the few photons in one short exposure that correspond to given spatial frequency $\mathbf{k}$ will be distributed over ~ 1000 detector pixels. The background count per pixel should thus be < 0.001/read, to be negligible compared to photon noise. This level should be achievable with the newly developed two-dimensional silicon CCD arrays with gain (Mackay et al. 2001). So far these detectors have been used for astronomy only in analog mode with modest gain and a noise equivalent to ~ 0.5 detected photons, to accommodate fluxes > 1 photon/pixel/read (Tubbs et al. 2002). But for our fluxes of $\ll 1$ photon/read they could be configured for true photon event detection. Operation at their maximum gain of 45,000 with a discriminator threshold set at $\sim 1000\ e^-$ would ensure nearly 100% photon event detection, with negligible background count rate from amplifier read noise of $\sim 100\ e^-$. Fast frame rates would be obtained by using a large number of small format devices read simultaneously at 10 MHz pixel rate.

2.4. Phase Accuracy When Only a Few Photons Are Detected

Once even a few photons are detected, speckle phase and amplitude may be derived (Goodman 1985). For each detector pixel registering position $\boldsymbol{\theta}$, wavelength λ and reference beam phase ϕ we assign a halo amplitude component

$$\frac{a(\boldsymbol{\theta},\lambda)}{a(0,\lambda)} = \frac{e^{i\phi}}{\sqrt{N(\boldsymbol{\theta},\lambda)N(0,\lambda)}} \tag{2}$$

if a photon is detected, and zero for no detection. Here $N(\boldsymbol{\theta},\lambda)$ is the average pixel count for the separate halo or reference beams, summed over the 4 phase channels. $N(0,\lambda)$ is the count for the same size pixel and wavelength bin centered on the star. The corrugation and intensity Fourier components of spatial frequency $\mathbf{k}$ derived from Equation 1 are then given by

$$\int e^{i\mathbf{k}\cdot\mathbf{x}} T(\mathbf{x}) \Delta z(\mathbf{x}) d\mathbf{x} = \frac{i}{4\pi}\frac{1}{n}\sum_n \lambda \left(\frac{a(-\boldsymbol{\theta},\lambda)^*}{a(0,\lambda)} - \frac{a(\boldsymbol{\theta},\lambda)}{a(0,\lambda)} \right) \tag{3}$$

and

$$\int e^{i\mathbf{k}\cdot\mathbf{x}} T(\mathbf{x}) \frac{\Delta I(\mathbf{x})}{2I} d\mathbf{x} = \frac{1}{2n}\sum_n \left(\frac{a(\boldsymbol{\theta},\lambda)}{a(0,\lambda)} + \frac{a(-\boldsymbol{\theta},\lambda)^*}{a(0,\lambda)} \right) \tag{4}$$

where the sum is taken over those n pixels of different wavelength that fall within the solid angle $2(\lambda/D)^2$ of the two diametrically opposite streaked speckles corresponding to $2\pi\boldsymbol{\theta}/\lambda = \pm\mathbf{k}$.

From numerical experiments modeling photon noise and speckle brightness fluctuations, we find that exposures in which the reference and halo levels each contribute on average only 3 photons to the summations of Equations 3 and 4 are already useful. The measurement accuracy is good enough to make a wavefront correction that will halve the intensity of typical speckles. If an unusually bright speckle contributes 12 photons, the intensity reduction will be improved to 2/3. No useful measurement and correction is obtained of faint halo regions averaging < 1 photon for the two speckles, but this does not matter.

Wavefront measurements at such low photon fluxes are made in practice with the most efficient current adaptive optics systems. Avalanche photodiodes are used to record single photons in the wavefront curvature sensor of the Hokupa'a AO system at the CFHT telescope (Graves et al. 1998). The measured threshold flux of 20,000 photons/sec total for wavefront improvement (tripling of Strehl ratio) corresponds to ~ 6 photons/subaperture per correction period of ~ 10 msec.

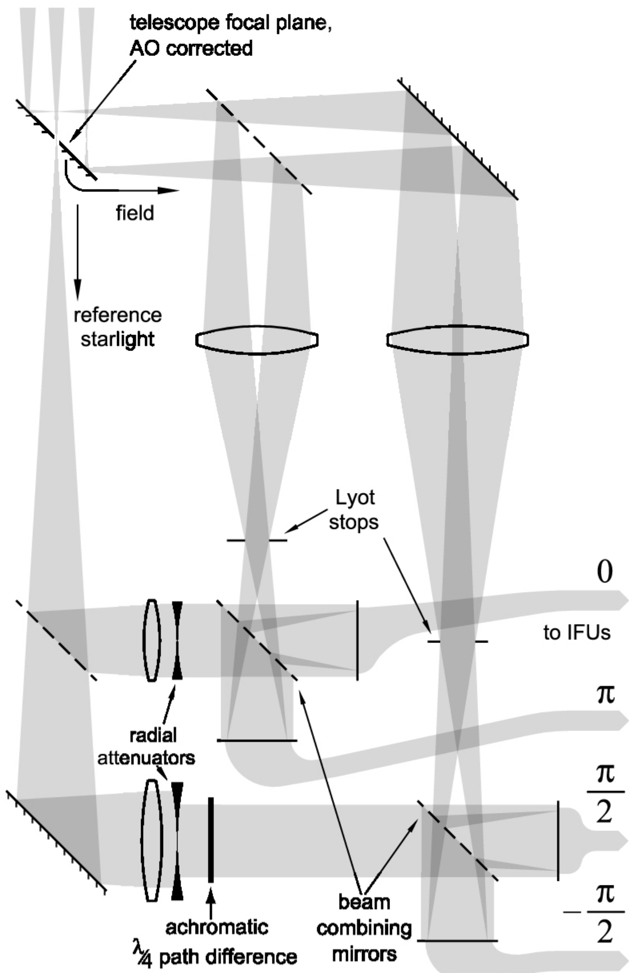

Figure 2. Schematic diagram of the coronagraphic interferometer. Light enters at top left at the telescope focus. The output images are relayed to integral field units (IFUs), not shown. (Drawing by Eric Anderson and Steve Spain.)

2.5. Comparison With Pupil Plane Sensing

At first sight, it might seem that higher accuracy wavefront correction might be achieved by conventional pupil plane measurements taking advantage of high photon fluxes. This is not the case. A self-referenced, phase shifting interferometer used to make pupil plane measurements and operating at the photon noise limit yields phase errors over individual sub-apertures of dimension Δx given by $\sigma^2 \simeq 4/(F^* q \Delta t \Delta x^2)$ (Angel 1994). Here F^* is the star photon flux, q is the overall photon detection efficiency (top of the atmosphere to detected photoelectrons) and Δt is the integration time. It follows from Equation 1 that corrections to the wavefront incorporating phase errors of this magnitude will lead to speckles of intensity $4/(AF^* q \Delta t)$ relative to the Airy core of the star, where A is the area of the wavefront. Since $AF^* q \Delta t$ is the number of photons recorded in the core, the number of photons recorded in the speckle will be ~ 4, independent of the number of photons used to measure the wavefront. This is essentially the same result as as for correction based on detection of just the few photons per speckle in the focal plane. The great advantage of focal plane measurement, as we have stressed above, is avoiding non-common path errors and the need for accurate calibration.

2.6. Wavefront Correction Elements

Wavefront corrugation and intensity aberrations will both be corrected, with two rapidly deformable mirrors conjugated to the primary and to a high atmospheric layer (Gonsalves 1997; Barchers 2002). The latter corrects scintillation, with displacements based on the Fienup phase retrieval algorithm (Roggemann & Lee 1997). The AO system must obtain high Strehl ratio, with $2\pi \langle \Delta z \rangle / \lambda$ and $\langle \Delta I \rangle / 2I << 1$ so Equation 1 is valid. An auxiliary pupil wavefront sensor measuring our bright target stars (R magnitude < 6) at $\lambda < 0.7$ μm should yield such accuracy. Atmospheric dispersion will be corrected both in the focal plane and at the high conjugated pupil.

To reduce the halo close to the star, the residual displacement and amplitude errors sensed by the coronagraphic interferometer will be used to fine tune the lower order corrections with unusually fast response time. It may be most practical to do this with auxiliary deformable mirrors with very fast response but modest resolution and small stroke. This is a dynamic version of a strategy suggested for coronagraphy with the Hubble Space Telescope, with a relatively small number of actuators used to overcome low order static mirror figure errors (Malbet et al. 1995). For example, the critical Fourier components for earth-like planet detection with 1 - 2 m wavelength at the entrance pupil (corresponding to 0.8 μm halo at $0.16 - 0.08$ arcsec radius) can be accurately reproduced by fast actuators with projected spacing of ~ 0.25 m. Residual fitting errors will be on a finer scale, resulting in higher order Fourier components that place energy beyond the search region. So as not to exacerbate the task of such fast, low-order correction, any slower deformable mirrors with higher resolution used in tandem should be moved smoothly, not in steps.

3. Performance Estimates

3.1. Correction of Kolmogorov Wavefront Distortion

To estimate the limiting sensitivity, we must quantify the character of the evolving wavefront, paying particular attention to its large amplitude, low-order components. The following simplified analysis includes only the dominant corrugation amplitude $z(\mathbf{x}, t, \lambda)$. A typical deformation is represented by a two dimensional Fourier series expansion (McGlamery 1976). Over aperture D, with wave numbers given by $k_{mx} = 2\pi m_x/D$ and $k_{my} = 2\pi m_y/D$ and the series summed over integers in the range $\pm m_{max}$, we have

$$z(\mathbf{x}, t, \lambda) = 0.7 \frac{n_\lambda}{n_0} \frac{\lambda_0}{r_0^{5/6}} \frac{1}{D} \Re \sum_m k_m^{-11/6} g_m e^{i(\mathbf{k}_m \cdot (\mathbf{x} - \mathbf{v}t))}. \tag{5}$$

Here r_0 is Fried's coherence length at wavelength λ_0. n_λ and n_0 are the refractive indices of air at the observed and reference wavelengths. The temporal evolution represents a single frozen layer with velocity $\mathbf{v}$. The $g_m(m_x, m_y)$ are Gaussian random numbers with real and imaginary components having zero mean and $\sigma = 1$. This formulation yields displacements valid over regions $\Delta x \geq D/m_{max}$. The pattern repeats for apertures $> D$ and underestimates the lowest order terms, but this is not important for our field of interest, $\theta \sim 15\lambda/D$.

Suppose that at one instant the atmospheric aberration is perfectly corrected, but thereafter the deformable mirrors remain fixed. After a short interval t the wavefront error is given by $t dz/dt$. It follows from Equations 1 and 5 that the halo intensity for ($\theta \leq \lambda/4vt$) is given by:

$$\frac{\langle I(\boldsymbol{\theta}, \lambda)\rangle_t}{I(0, \lambda)} = 0.7^2 \frac{\lambda_0^2}{r_0^{5/3}} \left(\frac{\lambda}{2\pi}\right)^{-1/3} \frac{1}{D^2} \left(v cos\phi_{\theta,v} t\right)^2 \theta^{-5/3}. \tag{6}$$

where $vcos\phi_{\theta,v}$ is the wind speed in the $\boldsymbol{\theta}$ direction and the intensities are in photons/ster/sec.

3.2. Optimum Correction Interval

Now consider a correction servo modeled as a series of instantaneous corrections made after exposures of length Δt, operating in a steady state in which an average total of 6 photons (3 each for halo and reference) are recorded for each speckle pair measuring spatial frequency $\mathbf{k}$. Based on our earlier discussion of photon noise, the speckle intensity will on average be halved after correction. Provided the residual errors after correction are random, Equation 6 describes the quadratic increase in halo intensity after each correction. Thus we can determine the optimum Δt by setting the projected halo photon count rate increase after time Δt, summed over the solid angle subtended by two speckles, equal to 3/Δt, i.e.,

$$\frac{\langle I(\theta, \lambda)\rangle_{\Delta t}\, 2(\lambda/D)^2}{I(0, \lambda)\,(\lambda/D)^2} = \frac{3}{F^* A S q \Delta t} \tag{7}$$

where we have normalized by the detected stellar photon flux in the central diffraction core, $I(0, \lambda)(\lambda/D)^2 = F^* A S q \Delta t$. Here S the Strehl ratio.

3.3. Limiting Sensitivity for Typical Atmospheric Conditions

As examples, we consider the sensitivity of 8 and 30 m telescopes in a band 0.85 ± 0.15 μm to the earth and jupiter (at 0.1 and 0.5 arcsec) in a solar twin at 10 pc, with $F^{*} = 3 \times 10^{8}/m^{2}/\text{sec}$. We take typical atmospheric parameters of $\lambda_0/r^{5/6} = 2.5 \times 10^{-6} m^{1/6}$ (corresponding to 0.7 arcsec visible seeing) and $v = 15$ m/sec. High throughput is crucial to performance, and every care must be taken to minimize losses. Based on the measured value of $q = 0.22$ for the Palomar IFU system (Murphy et al. 2000), we will assume $q = 0.15$. This allows for additional losses from AO elements and the apodization mask, and gains by using prism dispersion (instead of a grating and order filters) and very high efficiency coatings on all but the primary mirror. The AO system should achieve Strehl $S = 0.9$, corresponding to 70 nm rms wavefront error. With these parameters, and allowing for a small correction for chromatic wavefront errors from Equation 9 below, we find $\Delta t = 0.26$ msec for $\theta = 0.1$ arcsec and 0.65 msec for 0.5 arcsec, independent of aperture. Correction at such speeds should be possible: deformable mirrors with a 0.12 msec update rate have already been used in an Air Force AO system (Fugate 2002). The corresponding halo/star intensity ratios are 1.0×10^{-6} at 0.5 arcsec for D=8 m and 2×10^{-7} at 0.1 arcsec for D=30 m.

To minimize halo background, a planet will be detected in a single, centered spatial resolution element $d\Omega = (\lambda/D)^2$ that captures a fraction 0.75S of its flux at the detector. The number of planet photons detected in time Δt in is thus $0.75qSAF_p\Delta t$. In the same resolution element the (much larger) count for the halo plus reference beams averages 3 photons. Thus in a single exposure the S/N ratio (from photon noise alone) is $0.75qASF_p\Delta t/\sqrt{3}$. As we argue below, a tracking servo should result in speckle patterns effectively de-correlated from one exposure to the next, so the signal/noise ratio (S/N) will improve as $\sqrt{(T/\Delta t)}$, where T is the total integration time. Thus we obtain

$$S/N = 0.43qASF_p\sqrt{T\Delta t}. \tag{8}$$

For an earth-like planet ($F_p = 1.5 \times 10^{-10} F^{*}$), Equation 8 yields a signal/noise ratio of 5 for a 8-hour integration with D = 30 m. With such performance, a telescope of this aperture could be used to conduct a search for earth-like planets, with time for repeated observations of many candidate stars. For a jupiter twin ($F_p = 1.25 \times 10^{-9} F^{*}$) at 0.5 arcsec, the S/N ratio is 4.7 in 8 hours for D = 8 m, thus as the technique is developed it could be used to image known giant extrasolar planets with existing facilities. This sensitivity to giant planets is lower than for earlier estimates (Angel 1994; Stahl and Sandler 1995) because a more realistic throughput is assumed.

3.4. Predicting Wavefront Evolution

In practice, the above projections should be achievable or even exceeded, given a servo control algorithm that predicts wavefront evolution. The individual $\Delta z(t)$ components modeled by Equation 5 evolve smoothly on time scales $\tau = 1/\mathbf{k} \cdot \mathbf{v}$, typically 20 msec for $\theta = 0.1$ arcsec, much longer than Δt of 0.26 msec. $\Delta I(t)$ will evolve differently, but also smoothly. The measured Fourier components may show some faster variability, from cross coupling of higher order components by the pupil function. However this effect should be small, because $T(\mathbf{x})$ must be smoothly tapered for the k values of interest, to minimize diffraction. This suggests that the Fourier coefficients to be applied to the deformable mirror could be more accurately predicted with a tracking algorithm, rather than from just the last 6 photons measured in time Δt. The value of a predictive servo was recognized and explored in a numerical model by Stahl and Sandler (1995) for AO detection of a jupiter-like extrasolar planet. They found a filter using past history resulted in a more accurate correction than projected for a simple servo, and also almost completely removed the temporal correlation of successive wavefront errors. The latter is required if the halo is to average to a smooth background. Predictive tracking should be even more advantageous for terrestrial planet detection, because the critical $\mathbf{k}$ components have longer wavelengths and evolve more slowly, while Δt is shorter.

3.5. Imaging and Spectroscopy Longward of 1 μm

If a terrestrial planet is found, a spectrum will be of enormous interest. The above method automatically yields spectra with resolution $\lambda/\Delta\lambda \sim 50$, but the optical absorption features of water and oxygen from $0.7-0.9$ μm seen in Earth's integrated spectrum (Woolf et al. 2002) would be too weak to detect. However, strong water features are present from $1-2$ μm (DesMarais et al. 2001). The coronagraphic interferometer of Figure 2 could be built with dichroic mirrors between the Lyot stops and beam-combiners, directing wavelengths longer than 1 μm to additional integral field units with conventional infrared array sensors. Atmospheric dispersion will cause a halo at longer wavelength even when correction is perfect at the shorter sensing wavelength. From Equation 5 we find

$$\frac{\langle I(\theta,\lambda)\rangle_{\Delta n}}{I_0} = 0.7^2 \frac{\lambda_0^2}{r_0^{5/3}} \left(\frac{\lambda}{2\pi}\right)^{5/3} \frac{1}{D^2} \left(\frac{\Delta n}{n_0}\right)^2 \theta^{-11/3}. \tag{9}$$

The halo resulting from the index shift $\Delta n/n \sim 0.006$ for air between the corrected and imaged wavelengths will be comparable to that from servo error alone (Equation 6) but it will not be diluted by the reference beam. Water features at terrestrial level should be detectable in an exposure corresponding to a S/N ratio of 25 in the optical image, requiring $\sim$ 200 hours of integration with 30 m aperture. The $1-2$ μm region will also be of much interest for giant extrasolar planets where predicted strong spectral features (Burrows & Sudarsky 2003) could be observed with an 8 m telescope.

4. Discussion

Wavefront correction derived from focal plane sensing systems should make extrasolar planet detection practical from the ground. Even though the next generation of larger telescopes remains a decade or more away, it is important now to understand the technical issues, because the fundamental design choices being made now may have significant impact on limiting sensitivity. It is also important that, as alternative space missions for extrasolar planet detection are being considered, the relative potential capabilities of ground and space are understood.

4.1. Primary Mirror Configurations

Larger ground-based telescopes will require multiple primary mirror elements, which may be configured to synthesize a single aperture or as multiple apertures which can be combined coherently. Thus a variety of pupil transmission functions is possible, with different patterns of segmentation constraining $T(\mathbf{x})$ as well as the spatial scale of quasi-static discontinuities in $z(\mathbf{x})$. In making the sensitivity estimates above, we assumed single filled apertures with apodization that would not significantly reduce throughput and or degrade the diffraction limited image width. This is reasonable for continuous, unobscured mirror surfaces; for example, at 1 μm wavelength a search at 0.5 arcsec with an 8 m aperture or at 0.1 arcsec with a 30 m can be made with little apodization loss, because $\theta_p > 10\lambda/D$. For telescopes > 8 m, though, segmentation is unavoidable, and even for large individual segments $\theta_p < 5\lambda/d$. One way to optimize for extrasolar planet detection would be to build a large, off-axis, unobscured aperture from an array of very small segments. Provided these are regularly spaced, the PSF for the whole aperture will be free of diffraction peaks from the pattern of gaps, within a region of width λ/d (Born, Wolf & Bhatia 1999). If d=0.2 m, for example, the diffraction-free zone is 1 arcsec in radius. Segments of 2 m diameter (presently favored by the OWL designers) would seem to be the worst possible choice for terrestrial planet detection, as the gaps will scatter 1 μm light preferentially at 0.1 arcsec radius. Given that the technology for mass producing and controlling a huge and finely segmented adaptive mirror is not yet developed, a good choice today is to go to the other extreme, using a small number of the largest possible round segments, individually apodized. Angel et al. (2003) have shown that for a restricted radial zone as close as 0.05 arcsec from the star, again at 1 μm wavelength, suppression of 10^{-6} of the star peak can be achieved, given 8.4 m circular segments with annular apodizing masks removing 40% of the incident light. Observations could reveal many known giant extrasolar planets known at this angular separation, and predicted to show spectral peaks $> 10^{-8}$ of the star in the J band. (Burrows & Sudarsky 2003).

A large telescope built with two apertures and providing for coherent combination, such as the LBT (Hinz et al. 2001) or the proposed 20/20 telescope (Angel et al. 2003) opens additional possibilities for extrasolar planet detection, especially in the thermal infrared and for relatively bright planets too close to the star to be distinguished with a single apodized aperture. The two identically segmented or obscured stellar wavefronts would be superposed in a Bracewell interferometer with π phase difference. No apodization is required since the entire stellar PSF is suppressed. Residual atmospheric aberration in this case will cause the weak, nominally-canceled wavefront to have locally variable weak amplitude and phase. The advantages of corrections based focal plane interferometry can still be realized, if the reference beams are derived from the complementary, constructively-interfered wavefront.

4.2. Ground vs. Space

Atmospheric limitations could be mitigated to some extent by a high, dry site. Low water vapor will be particularly important if water features are to be detected in a terrestrial extrasolar planet. But only in space can atmospheric and thermal limits be avoided completely. A unique, complementary role will be for thermal observations with a cold Bracewell interferometer in the mid-infrared, where the contrast of terrestrial planets is much better, and where an Earth twin would show very strong features of ozone and carbon dioxide in addition to water (Angel, Cheng & Woolf 1996; Woolf 2003).

For optical detection, the advantage of space is not so certain; the inevitably smaller apertures will require higher accuracy wavefront control and more perfect apodization. To realize the full advantage for terrestrial planet detection, the diffracted and scattered stellar halo should be reduced to the 10^{-10} level of the planet. Apodization schemes to achieve such reduction at 0.1 arcsec are possible in principle for apertures ≥ 5 m ($\theta_p > 5\lambda/D$ at λ=0.5 μm) e.g., Nisenson & Papaliolios (2001). From Equation 1 we see that the relevant low order (~ 1 m wavelength) components of the wavefront must be actively controlled to an amplitude of a few picometers. The focal plane interferometric method described above gives the best chance of measurement to this accuracy. But at the 10^{-10} level, the time scale to collect a few photons per speckle will be a few minutes. The correction servo can thus run no faster than this rate, and stability against faster disturbances and vibration must be achieved at picometer levels without recourse to optical feedback.

Because of the large size requirement and extraordinary technical challenges of optical detection in space, it would be advantageous to use a telescope that can be assembled and modified in space. A concept for such an upgradeable and serviceable facility in low earth orbit is described by Angel & Codona (2002). But from the above discussion, it is clear that thermal creaking in the low orbit might be a major technical issue, and would need to be carefully studied. Thermal instability could be largely avoided in remote orbits, such as L2, but the inability to service the large and complex system would be a major drawback. Despite atmospheric aberration, new and larger mountaintop telescopes may in the end be more sensitive, if corrected to the limit we have described through evolutionary and developmental steps possible on the ground.

Acknowledgments. This paper has benefited from discussions with Nick Woolf and Johanan Codona, and careful reading of earlier manuscripts by Buddy Martin and two anonymous referees. This work is supported by grants AFOSR #F49620-01-1-0383 from the Air Force and AST-0138347 from the NSF.

References

Angel, J. R. P., Cheng, A. C. W. & Woolf, N. J. 1986, Nature, 322, 341

Angel, J. R. P. 1994, Nature, 368, 203

Angel, J. R. P., Burge, J., Codona, J. L., Davison, W., & Martin, H. 2003, Proc. SPIE, 4840, in press

Angel, J. R. P & Codona, J. L. 2002, *Hubble's Scientific Legacy: Future Optical and Ultraviolet Astronomy from Space*, (eds. K. Sembach, J. C. Blades, G. D. Illingworth & R. C. Kennicutt), ASP Conference Series

Barchers, J. D. 2002, J. Opt. Soc. Am. (A), 19, 54

Born, M., Wolf, E. & Bhatia, A. B. 1999, *Principles of Optics,* Cambridge University Press

Burrows, A. & Sudarsky, D. 2003, these proceedings

Close, L. M., Siegler, N., Potter, D., Brander, W. & Liebert, J. 2002, ApJ, 567 L53

Des Marais, D. J. et al. 2001, *Biosignatures and Planetary Properties to be Investigated by the TPF Mission,* JPL publication 01-008

Fugate, R. Q. 2002, private communication

Gonsalves, R. A. 1997, Optics Letters, 22, 588

Goodman, J. W. 1985, *Statistical Optics*, p. 500, (New York: Wiley)

Graves, J. E., Northcutt, M., Roddier, F., Roddier, C. & Close, M. 1998, Proc. SPIE, 3353, 34

Hinz, P. M., Angel, J. R. P., McCarthy, D. W., Hoffmann, W. F. & Woolf, N. J. 2001 *Science with the Large Binocular Telescope* (eds. T. Herbst & N. Druck), p. 203

Jacquinot, P. & Roizen-Dossier, B. 1964, Prog. Optics, 3, 29

Mackay, C. D., Tubbs, R. N., Bell, R., Burt, D. J., Jerram, P. & Moody, I. 2001, Proc. SPIE, 4306, 289

Malbet, F., Yu, J. W., & Shao, M. 1995, PASP, 107, 386

McGlamery, B. L. 1976, in *Image Processing.* (ed. J. C. Urbach), Proc. SPIE, 74, 225

Murphy, T. W. Jr., Matthews, K., & Soifer, B. T. 2000, *Imaging the Universe in Three Dimensions: Astrophysics with Advanced Multi-Wavelength Imaging Devices* (eds. van Breugel, W. & Bland-Hawthorn, J.), ASP Conference Series, 195, 200

Nisenson, P. & Papaliolios, C. 2001, ApJ, 548, L201

Perryman, M. A. C. & Peacock, A. 2000, *Imaging the Universe in Three Dimensions: Astrophysics with Advanced Multi-Wavelength Imaging Devices* (eds. van Breugel, W. & Bland-Hawthorn, J.), ASP Conference Series, 195, 487

Racine, R., Walker, G. H., Nadeau, D., Doyon, R. & Marois, C. 1999, PASP, 111, 587

Roddier, F. 1999, *Adaptive Optics in Astronomy,* Cambridge University Press

Roddier, C. & Roddier, F. 1993, Applied Optics, 32, 2992

Roggemann, M. C. & Lee, D. J. 1997, Applied Optics, 37, 4577

Smythe, R. & Moore, R. 1984, Optical Engineering, 23, 361

Stahl, S. M. & Sandler, D. 1995, ApJ, 454, L153

Thatte, N., et al. 2000, *Imaging the Universe in Three Dimensions: Astrophysics with Advanced Multi-Wavelength Imaging Devices* (eds. W. van Breugel & J. Bland-Hawthorn), ASP Conference Series, 195, 206

Tubbs, R. N., Baldwin, J. E., Mackay, C. D. & Cox, G. C. 2002, A&A, 387, L21

Woolf, N. J., Smith, P., Traub, W. & Jucks, K. 2002, ApJ, 574, 430

Woolf, N. J. 2003, these proceedings

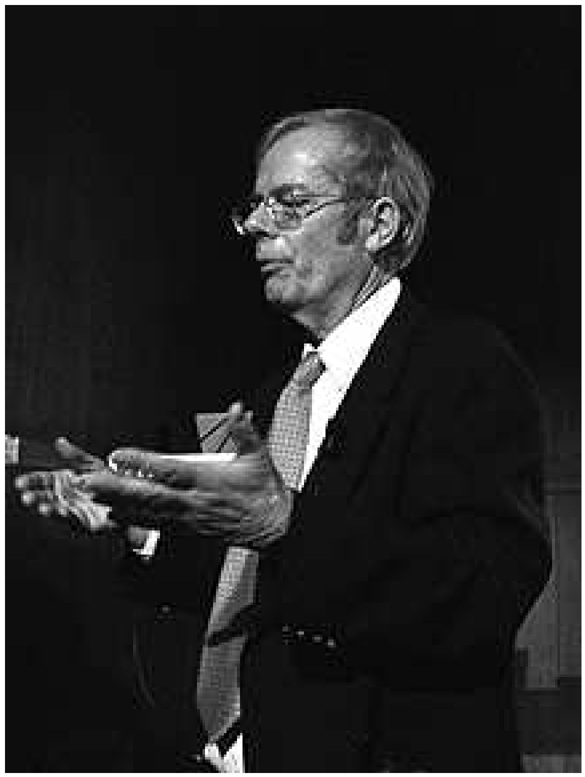

Roger Angel